Sp8 regulates inner ear development

Hyeyoung A. Chung, Sofia Medina-Ruiz, and Richard M. Harland[1]

Department of Molecular and Cell Biology, University of California, Berkeley, CA 94720-3200

Edited by Donald D. Brown, Carnegie Institution for Science, Baltimore, MD, and approved March 14, 2014 (received for review October 23, 2013)

A forward genetic screen of *N*-ethyl-*N*-nitrosourea mutagenized *Xenopus tropicalis* has identified an inner ear mutant named *eclipse* (*ecl*). Mutants developed enlarged otic vesicles and various defects of otoconia development; they also showed abnormal circular and inverted swimming patterns. Positional cloning identified *specificity protein 8* (*sp8*), which was previously found to regulate limb and brain development. Two different loss-of-function approaches using transcription activator-like effector nucleases and morpholino oligonucleotides confirmed that the *ecl* mutant phenotype is caused by down-regulation of *sp8*. Depletion of *sp8* resulted in otic dysmorphogenesis, such as uncompartmentalized and enlarged otic vesicles, epithelial dilation with abnormal sensory end organs. When overexpressed, *sp8* was sufficient to induce ectopic otic vesicles possessing sensory hair cells, neurofilament innervation in a thickened sensory epithelium, and otoconia, all of which are found in the endogenous otic vesicle. We propose that *sp8* is an important factor for initiation and elaboration of inner ear development.

The vertebrate inner ear is a sensory organ responsible for balance and sound detection. Dysfunction of the inner ear is among the most common congenital disorders, affecting at least 1 in 500 births (1) and ∼40% of sensorineural deafness is associated with inner ear malformations (2). However, the study of hearing and balance impairment in humans is limited by the inability to follow inner ear development. Vertebrates share similarities in the sequence of developmental events that form the inner ear: the formation of an otic placode from an ectodermal thickening, morphogenesis to form the otocyst, and regional patterning of the otic vesicle (OV), resulting in the 3D membranous labyrinth (3, 4). Multipotent sensory progenitor cells are induced in the ectoderm surrounding the anterior neural plate, a domain termed the preplacodal region (PPR), and *six1* has been characterized as marking this panplacodal domain. Signals from hindbrain and the regional expression of different transcription factors differentiate the PPR into the otic placode. The OV is partitioned by asymmetrical expression of various developmental regulators to pattern subdomains of the developing inner ear.

The abilities of *Xenopus* to elucidate the cellular and molecular aspects of developmental processes position it as a valuable model organism (5–7). Earlier studies of lineage analysis and spatiotemporal expression of transcription factors during inner ear development led to construction of an inner ear fate map in *Xenopus* and this fate map allows us to interpret gene expression patterns within the context of the anatomy (8, 9). In recent years, genetic and genomic approaches have been developed in *Xenopus tropicalis* (10–13). To advance our understanding of inner ear development, we have screened *N*-ethyl-*N*-nitrosourea (ENU) mutagenized *X. tropicalis* colonies and recovered an inner ear mutant named *eclipse* (*ecl*). The *ecl* mutant perturbs *specificity protein 8* (*sp8*) expression and leads to aberrant sensory organ development, uncompartmentalized and enlarged OVs, and otoconial defects. The zinc-finger transcription factor *sp8* is related to *Drosophila buttonhead*. In mice, mutation of *sp8* caused severe truncations of the limbs and tail and defective brain and abnormal olfactory development (14–17). Limb/fin outgrowth in chick and zebrafish embryos also employs *sp8* (18), suggesting the conserved function of *sp8* across phylogeny. In *Xenopus*, the gene was identified as a target of *sox17* (19). Here, we demonstrate a role for *sp8* in inner ear development.

Results

In a screen of ENU-mutagenized *X. tropicalis*, we identified *eclipse* mutants. Mutant tadpoles were usually immobile and often swam upside down or in circles, whereas WT tadpoles actively swam with a dorsal-up position and linear trajectory, suggesting swimming and balance defects in the mutants. When the culture dish was tapped, a WT embryo responded quickly and swam, whereas the mutant showed a slower response (Movies S1 and S2). Mutant embryos developed normally until the mid-20 stage but showed enlarged OV from stage 28. By stage 40, the gross external phenotypes of mutants are comparable to those of WT siblings but various inner ear defects including enlarged OV and complete or partial loss of otoconia are seen in *ecl* embryos (Fig. 1 *A*–*C*). At stage 45, when otoconia are mature, the following otoconial defects were observed: devoid of otoconia, reduced otoconia, or scattered otoconia (Fig. 1 *A′*–*C′*). We classified the *ecl* phenotypes into three classes: *ecl 0*, with two inner ears of enlarged OV and no otoconia; *ecl 1*, with enlarged OV and devoid of otoconia on one side ear and a relatively normal size of OV with otoconia defects on the other side; and *ecl 2*, with two inner ears with otoconia defects but relatively normal OV size (Fig. S1). After feeding stage 45/46, *ecl* embryos declined rapidly and never reached metamorphosis. To determine the genetic lesion in *ecl* mutants, we genotyped genomic DNA from mutants and WT siblings using published or self-designed simple sequence-length polymorphism (SSLP) markers (11, 20). Linkage analysis using pools of genomic DNA from gynogenetic mutants and WT siblings assigned the *ecl* mutation to linkage group 6 (LG6) (old LG2), corresponding to scaffold 6 in *X. tropicalis* genome assembly 7.1 (www.xenbase.org) (Fig. S2). We genotyped ∼4,000 F3 *ecl* tadpoles from a mapcross and placed *ecl* between two flanking markers of 25B04 and SSLP 52.5, an interval of 353.2 kb (Fig. 1*D*). We further generated an

Significance

Deficits in hearing or balance are common and result from both developmental and environmental causes. Model organisms have contributed many fundamental insights into embryonic development and we have added *Xenopus tropicalis* as a new genetically tractable organism in the field of inner ear development. As a result of a forward genetic screen in *X. tropicalis*, we have identified *specificity protein 8*, a new initiator of ear development, and analyzed mutant phenotypes and molecular interactions with genes that are involved in inner ear development. Given morphological and genetic similarities between inner ears of frog and mammals, the establishment of a new in vivo model system amenable to genetic manipulation will provide an important new tool to study vertebrate ear development.

Author contributions: H.A.C. and R.M.H. designed research; H.A.C. performed research; H.A.C., S.M.-R., and R.M.H. analyzed data; and H.A.C. and R.M.H. wrote the paper.

The authors declare no conflict of interest.

This article is a PNAS Direct Submission.

Data deposition: The sequence of sp8 mRNA reported in this paper has been deposited in the GenBank database (accession no. KJ158464).

[1]To whom correspondence should be addressed. E-mail: harland@berkeley.edu.

This article contains supporting information online at www.pnas.org/lookup/suppl/doi:10.1073/pnas.1319301111/-/DCSupplemental.

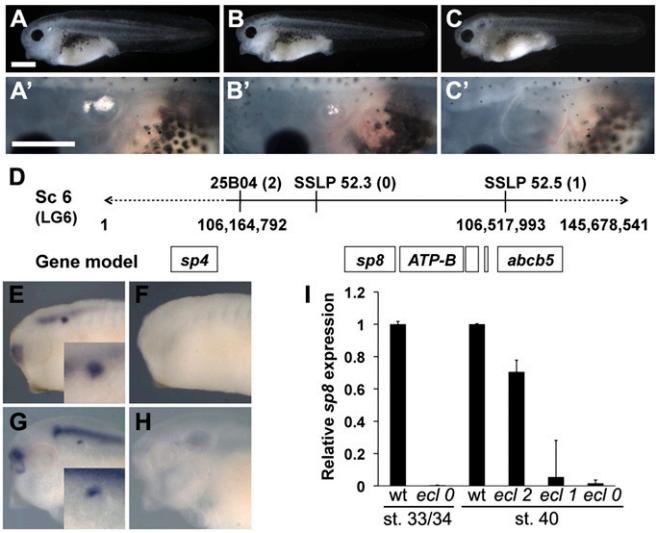

Fig. 1. *Sp8* mRNA is reduced in *ecl* mutants. Gross morphology at stage 40 in WT (*A*) and *ecl* mutants (*B* and *C*). The inner ears in WT (*A*′) and mutants (*B*′ and *C*′) at stage 45. (Scale bar, 500 μm.) (*D*) Mapping interval of *ecl* mutants on the scaffold/chromosome 6. Parentheses indicate numbers of recombinants from 4,000 genotyped *ecl* tadpoles. Whole-mount in situ hybridization in WT (*E* and *G*) and *ecl* mutants (*F* and *H*). (*Upper*) Stage 26; (*Lower*) stage 33/34. (*Inset*) *sp8* expression pattern in the OV of WT embryos. (*I*) qPCR analysis in WT and *ecl* embryos at stages 33/34 and 40. Error bars indicate SEM.

intervening SSLP 52.3 marker and confirmed the mapping interval of *ecl*. The predicted gene models in the published assembly include *specificity protein 8*, *ATP-binding cassette subfamily B*, *hypothetical protein*, and *putative hydrolase*. Among these genes, *sp8* is transiently expressed in the OV in mouse embryos (15) so we analyzed expression patterns of *sp8* in *X. tropicalis* by in situ hybridization in WT and mutant embryos. As also reported for EST10 (19), staining for *sp8* mRNA was found in the olfactory bulb, midbrain, hindbrain, and the OV in WT embryos, whereas no such signals were detected in *ecl* mutants (Fig. 1 *E*–*H*). Interestingly, *sp8* is expressed in the entire OV at early stages but becomes dorsally restricted in the OV at stage 33/34. Quantitative PCR analysis revealed that expression of *sp8* in mutants was drastically reduced compared with WT siblings at stage 33/34 and at stage 40. Compared with the expression of *sp8* in WT at stage 40, there was ∼30% and 95% reduction of *sp8* expression in *ecl 2* and *ecl 1*, respectively, (Fig. 1*I*). A more extreme difference was found in RNA-sequence data using dissected OVs of WT and *ecl 0* embryos at stage 37 ($2{,}772/10^8$ versus $1.45/10^8$ reads, respectively, for *sp8* in WT and *ecl 0*). To identify the specific lesion in *ecl* mutants, we sequenced the *sp8* genomic region in WT and mutant embryos. However, we failed to find changes in coding sequence or splicing signals, suggesting that the mutation might lie in a gene regulatory element. We therefore resequenced the genome and compared *ecl* mutant to WT genomes or the *X. tropicalis* reference genome assembly. Although several promising SNPs have been identified around 20 kb upstream of the start site, and these lie in a conserved region, we have not yet confirmed that any are responsible for the phenotype. Nevertheless, the variable expression of *sp8* and variable penetrance of the phenotype are consistent with a regulatory mutation that stochastically affects expression.

Database searches showed that homologs of *X. tropicalis sp8* are well conserved from *Drosophila* to human but different isoforms are reported (21). To characterize *sp8* transcripts in *X. tropicalis*, we carried out 5′ RACE. The sole *sp8* transcript identified here predicts a conserved protein of 520 amino acids with the specificity protein domain, buttonhead box domain, and zinc-finger domains (Fig. 2*A*). To verify that *sp8* is the affected gene in *ecl* mutants, we injected an *sp8* translation blocking MO (*sp8* ATGMO) bilaterally at the two-cell stage; this elicited an enlarged OV, absence or partial defects of otoconia with different penetrance among injected embryos, and circular/ventral swimming patterns, all of which are characteristic of *ecl* mutants (Fig. 2*F* and Fig. S3). A standard control MO (Con MO) did not show any effects. The inner ear defects induced by *sp8* ATGMO can be partially restored by the addition of a rescuing form of *sp8* mRNA, which also phenocopied *ecl* mutants when overexpressed. This experiment indicates that Sp8 is depleted in a gene-specific manner by ATGMO and the precise level of Sp8 is important for proper ear development. In addition, a splice-blocking MO (SBMO) also phenocopied inner ear defects found in the mutants (Fig. S3). These gene knockdown and rescue results confirm the requirement of *sp8* in inner ear development, supporting the genetic mapping and expression results that *sp8* is reduced or eliminated in the *ecl* mutant.

The availability of targeted genome editing methods such as zinc-finger nucleases (ZFNs), and transcription activator-like effector nucleases (TALENs) permits independent mutations to be made in genes of interest (22, 23). Inner ear defects in *sp8* TALEN-injected embryos can be observed from stage 28 and we classified TALEN-induced phenotypes as for *ecl* mutants (Fig. 2 *B*–*E* and *G*). Compared with the uninjected controls, *sp8* TALEN-injected embryos showed abnormal swimming and startle behavior at the swimming tadpole stage (Movie S3), with a dose-dependent severity (Fig. 2*G*). *Sp8* TALEN also elevated the penetrance of mutant phenotypes from matings of *ecl* heterozygotes. *Sp8* TALEN-injected embryos will undergo double-strand breaks (DSBs) at the TALEN target sites and the repair of DSBs can lead to a spectrum of indels within this region. To

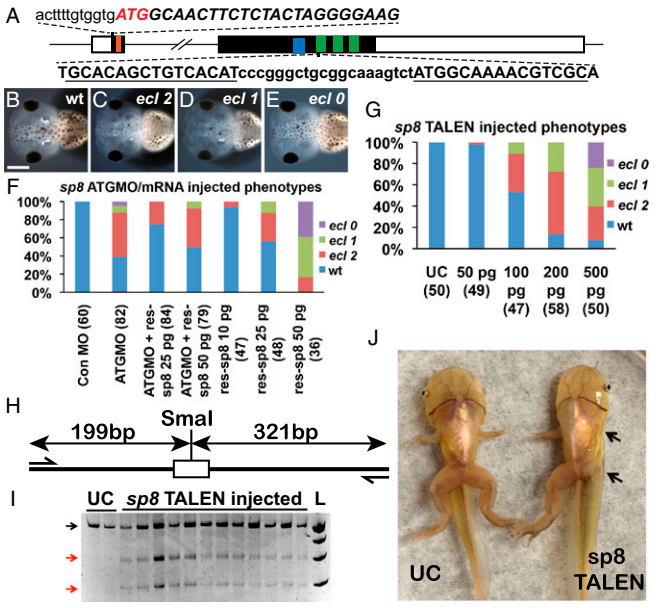

Fig. 2. Depletion of Sp8 by MO and TALEN phenocopy *ecl* mutants. (*A*) *Sp8* gene model and sequences of MO and TALEN target. Translation start site is marked in red. Sequences of MO, 5′ UTR, and TALEN binding sites are denoted in italic uppercase, lowercase, and underline, respectively. Domains of Sp, buttonhead box, and zinc finger are colored orange, blue, and green, respectively. (*B*–*E*) Phenotypes of *sp8* TALEN-injected embryos. (*F* and *G*) Phenotypes of *sp8* MO-, mRNA-, and TALEN-injected embryos. Number of injected embryos is shown in parentheses. (*H*) *sp8* TALEN target amplicon and Cel1 target. (*I*) Cel I assay for nonhomologous end joining events induced by *sp8* TALEN. Red arrows indicate mismatch cleavages due to mutation at the target. L is the DNA size marker. (*J*) Regional injection of *sp8* TALEN leads to loss of limbs. UC, uninjected control.

characterize TALEN-induced mutations at targeted *sp8* loci, we amplified genomic DNA fragments of 520 bp from *sp8* TALEN-injected individuals (Fig. 2*H*) and used CEL I endonuclease as previously to detect mutations induced by ZFNs (22). The CEL I assay produced two smaller fragments of ∼200 bp and 300 bp, respectively, only in *sp8* TALEN-injected individuals, whereas only a larger fragment of 520 bp was found in controls (Fig. 2*I*). Even injected embryos with a WT inner ear structure showed evidence of cleavage, suggesting nearly all *sp8* TALEN-injected embryos contain targeted mutations. We sequenced PCR amplicons and identified a wide range of variants at the targeted region from small to large deletions, insertions, or combined indels (Fig. S4), consistent with previous reports (23). We also found multiple different mutant alleles in genomic DNA isolated from single embryos. These observations confirm that *sp8* TALEN induces independent mutations in different cells of injected embryos during embryogenesis and further substantiates the identity of *sp8* as the affected gene in *ecl* mutants. In the mouse, the *sp8* mutant lacks limbs (14, 15). Although *ecl* homozygotes do not survive, the mosaic nature of TALEN-induced mutations suggests a way to observe later defects in *Xenopus*. Indeed, unilateral injection of TALEN at the two-cell stage allowed survival of tadpoles to metamorphosis ($n = 25$, starting from $n = 98$) and in many cases these animals lacked limbs on the injected side ($n = 16$) (Fig. 2*J*). We also made TALENs to target candidate regulatory sequences near *sp8* (Fig. S4). Compared with the *sp8* TALEN that targets the coding region, each of these TALENs induced only moderate inner ear phenotypes. Thus, the enhancer activity is probably distributed and we cannot specify with certainty which region is associated with the *ecl* mutation.

The inner ear is a membranous labyrinth whose fluid-filled tubes and chambers facilitate senses of hearing and balance. In vertebrates, the spherical OV undergoes extensive invaginations of the vesicle walls to form a multichambered inner ear with vestibular and auditory end organs (24). Wax sections, stained with hematoxylin and eosin (H&E), showed the initial compartmentalization of the utricle, horizontal canal, and sacculus in WT embryos at stage 46/47. In anterior sections, the thickening of lateral membrane in the utricular compartment indicates the initial structure of anterior canal cristae, with otoconia located near the utricular membrane (Fig. 3*A*, arrow). In middle sections,

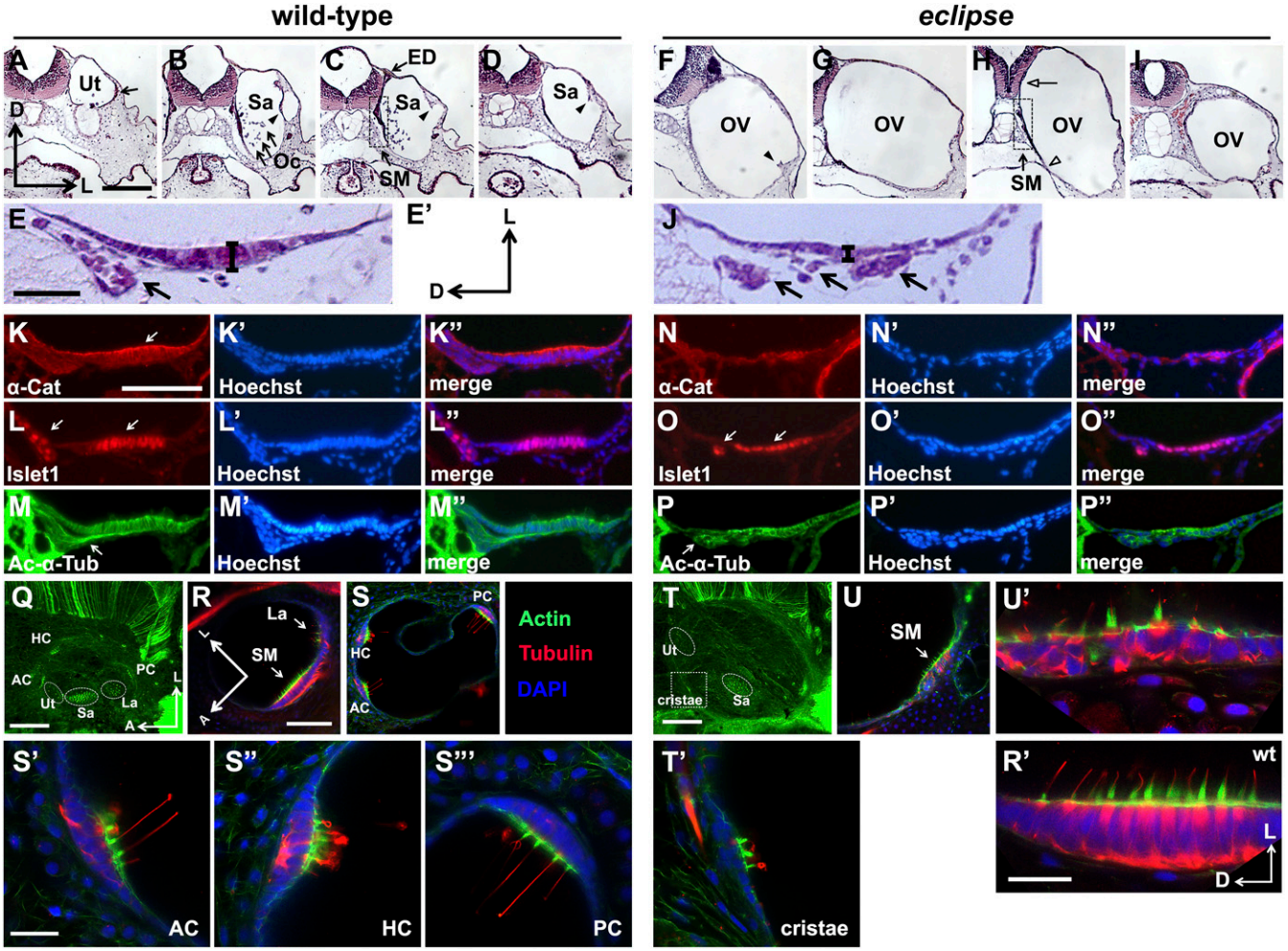

Fig. 3. Inner ear development is aberrant in *ecl* mutants. (*A–J*) H&E staining of wax-embedded WT and *ecl* embryos at stage 46/47. (*A* and *F*) Anterior, (*B*, *C*, *G*, and *H*) middle, and (*D* and *I*) posterior sections. (Scale bar, 100 μm.) (*E* and *J*) SM in WT and *ecl*, respectively. (Scale bar, 25 μm.) Black arrows and bar indicate CVG and the thickness of SM, respectively. (*E′*) Image position of *E* and *J*. Immunofluorescence for α-catenin (*K–K″* and *N–N″*), Islet 1 (*L–L″* and *O–O″*), and acetylated-α-tubulin (*M–M″* and *P–P″*) in WT and mutants, respectively. (Scale bar, 50 μm.) (*K′*, *L′ M′*, *N′*, *O′*, and *P′*) Hoechst staining and (*K″*, *L″*, *M″*, *N″*, *O″*, and *P″*) merged images. (*Q* and *T*) Staining of actin in WT and *ecl* OVs at stage 46/47. (Scale bar, 100 μm.) (*R*, *S*, and *U*) Sensory hair cells of the saccule and the cristae in WT and mutant embryos. (Scale bar, 100 μm.) (*R′*, *S′–S‴*, *T′*, and *U′*) Hair cells of the saccule and the cristae in WT and mutant OVs. (Scale bar, 25 μm.) Compare *U′* and *R′* for SM staining. Ut, utricle; Sa, saccule; Oc, otoconia; ED, endolymphatic duct; AC, anterior cristae; HC, horizontal cristae; PC, posterior cristae; La, lagena; and SM, saccular macula.

the protrusion of the vesicle wall leads to separation of saccule and horizontal canal (Fig. 3 *B* and *C*, arrowhead). Previous studies demonstrated that the extensive invaginations and fusion of these vesicle membrane protrusions give rise to the formation of semicircular canal (SCC) compartments (24–26). A saccular macula (SM), cochleovestibular ganglion (CVG), otoconia particles in the saccule, and endolymphatic duct (ED) are visible in these sections. CVG cells are present between the OV and hindbrain. The protrusion of the vesicle wall is still obvious in the posterior section (Fig. 3*D*, arrowhead). In the *ecl* mutant, however, there is only a small membranous protrusion (Fig. 3*F*, arrowhead); the inner ear remains as a single large vesicle with no otoconia particles or ED (Fig. 3 *F–I*). Due to enlarged OV, the neural tube is compressed toward the medial axis (Fig. 3*H*, open arrow) and the OV and archenteron wall even touch, with no intervening cartilage (Fig. 3*H*, open arrowhead). More strikingly, the SM was extremely thin and the CVGs were dispersed, in contrast to those of WT, which are clustered together between the hindbrain and SM (Fig. 3 *E* and *J*). These observations are consistent with increased volume and pressure of OV fluid, in addition to disorganization of the sensory structures.

To address the structure of sensory organs, we examined the distribution of cell membranes, sensory ganglia, and end organ innervation. Cryosections were taken from WT and mutant embryos at stage 45. In WT embryos, α-catenin, localized to adherens junctions in columnar sensory epithelium (27), was enriched in the apical membrane of SM (Fig. 3 *K–K″*, arrow). However, apically biased distribution of α-catenin was not detected in mutant embryos and otic epithelium failed to establish a columnar morphology, indicating that the tissue integrity is lost in mutant SM (Fig. 3 *N–N″*). Next, we examined CVG and neurofilament development. In WT, we found that Islet1 marks auditory and vestibular neurons in CVG, between the hindbrain and OV, as well as in cells within the SM (Fig. 3 *L–L″*, arrows). In *ecl* mutants, Islet1-positive CVG cells are not positioned properly and the number of Islet1-expressing cells is reduced by ∼60% (Fig. 2 *O–O″*, arrows and Fig. S5). Highly organized neurofilament-positive sensory projections into the CVGs and the SM are evident in WT embryos, whereas these projections immunostained by acetylated-α-tubulin antibody are misrouted around the SM in mutants (Fig. 3 *M–P″*, arrows). Although we observed apical accumulation of tubulin in some cells of SM and protrusions from these cells in WT, these are largely absent in mutant embryos. Abnormal distribution of these proteins due to *sp8* down-regulation indicates that the neuronal connection of the inner ear into the central nervous system was functionally impaired in *ecl*. We further observed sensory hair cell patches in whole embryos or dissected OVs using confocal microscopy. The actin-rich stereociliary bundles and kinocilium of mechanosensory hair cells that are important to detect sound and gravity were visualized with Alexa-conjugated phalloidin, a probe of F-actin, and actetylated-α-tubulin antibody, respectively. In the inner ear, stereociliary bundles can be observed by stage 31 (24). Sterociliary bundles are readily stained in sensory end organs of the utricle, saccule, and three cristae by stage 45, and lagena at stage 46/47 in WT embryos. Basal accumulation of actin in the stereociliary bundles of these sensory end organs, and perpendicular protrusions of stereociliary bundles from the basal membrane are observed in WT OVs (Fig. 3 *Q–S‴*). The kinocilia in the three cristae can be easily visualized at this stage. To our surprise, we failed to detect any of these in the cristae of *ecl* mutants, or in *sp8* ATGMO- or *sp8* TALEN-injected embryos at stage 45. By stage 46/47, hair cells in the utricle, saccule, and cristae were not only reduced in numbers but also developed abnormally in shape in *sp8*-depleted embryos (Fig. 3 *T–U′*). No lagena was found in these embryos. Whereas we observed stereociliary bundles, kinocilia, and thickened epithelium in all three cristae of WT embryos, we could only detect partially developed and multidirectional stereociliary bundles in the cristae of *sp8*-reduced embryos.

Although previous studies have shown that *sp8* is important during embryogenesis, it is unknown how *sp8* regulates inner ear development. The expression of *six1* was examined to determine whether *sp8* affects PPR development. *Six1* expression in PPR was unchanged in *sp8*-depleted embryos compared with uninjected controls (Fig. S6). We assessed hindbrain patterning, especially focusing on rhombomere (r)3–6, adjacent to the developing inner ear. At stage 18, *krox20* and *epha4* were normally expressed in r3 and r5 in uninjected control embryos. In TALEN- or MO-injected sides, r5 expression of *krox20* and *epha4* was reduced, especially near the presumptive otic placode (Fig. 4 *A–D*). As in mice (28), *mafb* is expressed in r5 and r6 in *X. tropicalis* embryos. In TALEN- or MO-injected embryos, the *mafb* expression domain was elongated laterally and especially expanded in the future otic territory (Fig. 4 *E* and *F*). *Gbx2* expression was increased on the injected side (Fig. 4 *G* and *H*). A posterior shift of *gbx2* expression was observed, consistent with the previous study of *sp8* as a midbrain–hindbrain boundary regulator (16). Although the *ecl* mutation did not show the severe head defects reported for the mouse, these expression analyses reveal that *sp8* still has a conserved function to regulate brain development. We examined *foxj1.2* expression in TALEN-injected embryos and uninjected control embryos. *Foxj1.2* expression was detected in the presumptive OV, as previously reported in *X. tropicalis* and zebrafish embryos (29, 30), and this expression was reduced on the *sp8* TALEN-injected side (Fig. 4 *I* and *J*), suggesting *sp8* regulates hair cells via *foxj1* and the hair cell defects found in *sp8*-reduced embryos are likely to be primary effects. We then examined markers of ear development (Fig. 4 *K–T*). *Pax2*, whose function along with *pax8* is critical for otic placode formation and cochlear and vestibular development (31, 32), was expressed in the whole OV with strong dorsomedial expression in WT but its expression was reduced in mutants. We also observed loss of *pax2* expression in TALEN- or MO-injected embryos at stage 19/20 embryos and these findings are similar to the effects of loss of *sp5* in zebrafish (33). *Msx1*, implicated in ED formation (26), is restricted to the dorsal part of the OV in WT, whereas this dorsal expression was absent in mutants. Notably, *sp8* expression is also restricted to the dorsal OV and overlapped with *msx1* expression.

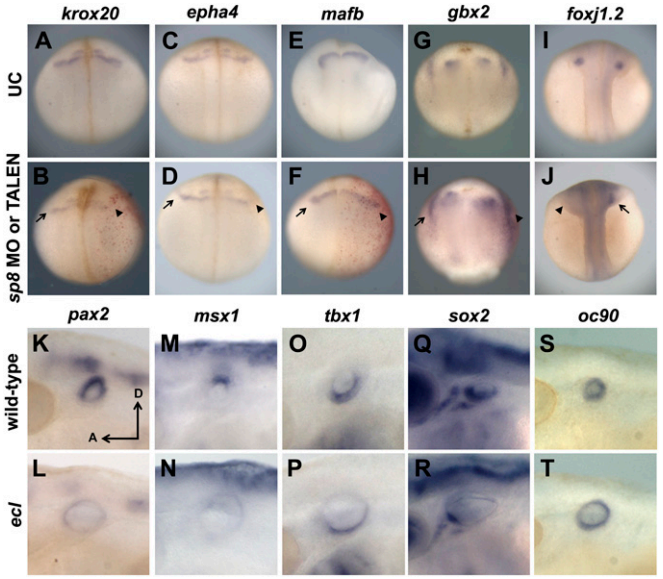

Fig. 4. Molecular markers of the inner ear in *sp8* MO- or TALEN-injected embryos. (*A–J*) Expression patterns of *krox20*, *epha4*, mafb, *gbx2*, and *foxj1.2* in uninjected and *sp8* TALEN- or MO-injected embryos. Arrows, uninjected side. Arrowheads, injected side. Anterior is up. (*K–T*) Expression domains of *pax2*, *msx1*, *tbx1*, *sox2*, and *oc90* in WT and mutant embryos at stage 33/34.

Ventroposterior expression of *tbx1* within the OV in WT was not significantly changed in mutants despite expansion of OV. *Sox2* is required for hair cell development (34) and its ventromedial expression was reduced in *ecl* mutants. The otoconia matrix protein marker, *oc90*, was expressed in the entire OV membrane of WT embryos. No changes in *oc90* expression were found in mutant OV, even though no otoconia were observed in this class of *ecl* mutants. No significantly increased cell death or cell proliferation was detected in mutant embryos (Fig. S7). These data suggest that the regional information of the OV is partially altered and that dorsal patterning was particularly perturbed in the *ecl* mutant.

Embryos receiving a high dose of *sp8* mRNA showed a reduced head and tiny eyes, although we often observed either enlarged or reduced OVs in these embryos. A lower dose of *sp8* mRNA can induce additional OV near the endogenous OV (Fig. 5 *A–D*). Most ectopic OVs possessed otoconia but were smaller in size compared with the endogenous OV. Of injected embryos (n = 118), ectopic OVs are observed in ∼16% of embryos. Expression of *pax2* and *oc90* was assessed to explore inner ear formation in earlier stages and to characterize subtler phenotypes. At stage 28, we observed different classes of aberrant *pax2* and *oc90* expression in *sp8* mRNA-injected embryos in comparison with control embryos (Fig. 5 *E–H*). Domains of *pax2* expression were ectopic (22%), expanded (13%), reduced (18%), and compound (7%) in tested embryos (n = 132). Similar results were obtained when *oc90* expression was examined. Although it was hard to detect more than one ectopic OV at stage 44/45, multiple ectopic microvesicles were often seen. These additional placodal domains were located around the head with various locations anterior to ventral or dorsal but very rarely posterior to the endogenous OV. The expression domain of *pax2* in hindbrain is also expanded in some embryos (n = 5). Other ectopically expressed or up-regulated genes include *sox2*, *msx1*, and *neurod* (Fig. S6), suggesting that these genes are downstream targets of *sp8*. We conclude that the gain of function of *sp8* can expand the endogenous domain of the otic placode and is sufficient to induce otic development elsewhere in the otic placodal territory. Transient activation of Fgf signaling and misexpression of *pax2* or *pax8* with Fgf signaling led to production of ectopic otic tissues in zebrafish (35). To test whether *sp8* might interact with these factors in the commitment of cells to the otic fate, we used *oc90* expression as a marker of differentiated otic tissue. Compared with a single injection, *sp8*/*pax2* coinjection increased the frequency of ectopic *oc90* expression but the domain of *oc90* expression more frequently became enlarged at higher sp8/pax2 coinjection (Fig. S8). *Sp8*/*pax8* coinjection resulted in reduction of *oc90* expression. *Sp8*/*fgf8* coinjection more frequently reduced *oc90* expression than single injections of *sp8* and *fgf8*. *Sp8* can interact with these factors in otic development but their individual and combined contributions to otic development defies a simple interpretation.

The findings that gain of *sp8* function can induce not only ectopic OVs but also molecular markers of the inner ear, such as *pax2* and *oc90*, led us to investigate ectopic OV development further. An extreme case of a ventral ectopic vesicle, developing adjacent to cranial cartilage, was examined by histology. This ectopic vesicle was surrounded by filamentous structures at the ventromedial position (Fig. 5*M*). A regionally thickened SM-like structure was also observed in sections (Fig. 5*N‴*). To examine mechanosensory hair cells and neurofilament innervation by confocal microscopy, phalloidin and antiacetylated-α-tubulin were used as before. This approach demonstrated the presence of both kinocila and innervation in the ectopic OV (Fig. 5 *N–N‴*), confirming that *sp8* is sufficient to induce fully differentiated inner ear structures within the placodal field. Wnt signaling is known to regulate *sp8* expression in the limb (18). To determine whether this is similar in inner ear development, embryos were treated from stage 13 to stage 28 with 6-bromoindirubin-3′-oxime (BIO), a Wnt agonist, which inhibits GSK3β-mediated degradation of β-catenin (36). At stage 28, we observed increased or ectopic *sp8* expression domains in treated embyos, compared with untreated embryos and the expression level of *sp8* was increased by BIO treatment (Fig. 5 *O–Q* and *T*). Increased or ectopic *oc90* expression was also observed in BIO-treated embryos and these changes were reversed when *sp8* was depleted (Fig. S9). We asked next whether inhibiting canonical Wnt signaling affects *sp8* expression. We unilaterally injected 80 pg of *dkk1*, an extracellular Wnt antagonist, at the two-cell stage, and analyzed *sp8* and *oc90* expression. We observed down-regulation of *sp8* expression but not *oc90* expression in the presumptive OV compared with the control embryos (Fig. 5 *R* and *S* and Fig. S9). These data indicate Wnt signaling has a conserved and selective role in *sp8* expression.

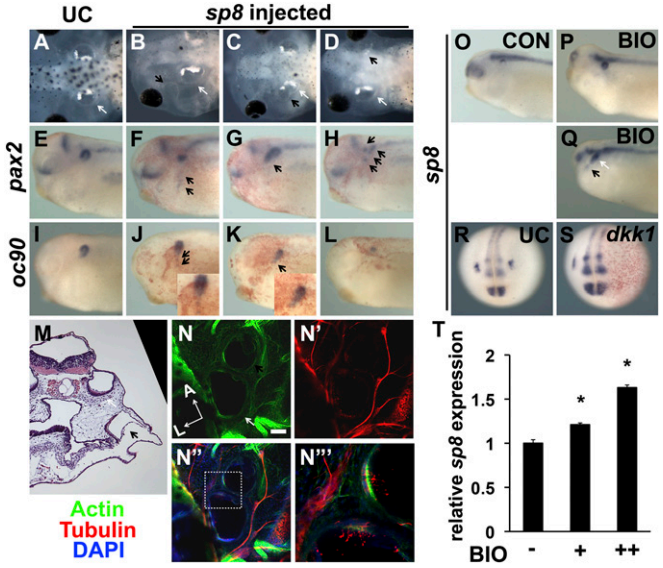

Fig. 5. *Sp8* can induce ectopic OVs. (*A–D*) Bright field images of the inner ear at stage 45 in control and *sp8* mRNA-injected embryos. Expression of *pax2* (*E–H*) and *oc90* (*I–L*) at stage 28. (*M*) H&E staining of *sp8*-injected embryos possessing ectopic OV. (*N–N‴*) Confocal images of ectopic OV stained with phalloidin 488, antiacetylated-α-tubulin antibody, and merged image. *Inset* is enlarged image of SE and hair cells in the ectopic OV. (Scale bar, 100 μm.) (*O–S*) Expression patterns of *sp8* in BIO-treated or *dkk1*-injected embryos. (*T*) qPCR analysis of *sp8* expression for BIO-untreated or 1 μM (+) and 10 μM(++) treated embryos. Error bars indicate SEM, $*P < 0.05$ between BIO-treated and control-treated embryos. Black arrows, ectopic OVs; white arrows, endogenous OVs.

Discussion

In this study, we have characterized a novel function of *sp8* during inner ear development (Fig. 1). Although we could not find the specific lesion in the *eclipse* locus here, genome modification by TALEN and MO knockdown of *sp8* function phenocopied the mutation, providing confidence that *sp8* disruption is the cause of the *ecl* phenotype (Fig. 2). We demonstrate that *sp8* is sufficient to induce ectopic OVs possessing differentiated sensory organs (Fig. 5). Recent studies showed that either activation of Wnt signaling or transient inactivation of Bmp signaling can lead to ectopic digit/fin formation in other vertebrates and increased *sp8* expression was evident in both situations (18, 37). Although *ecl* mutants did not survive until metamorphosis, we found that embryos injected unilaterally with *sp8* TALEN showed limb outgrowth defects (Fig. 2*J*) and this finding supports a conserved function of *sp8* in the limb context. Similarly, it is likely that conserved functions of *sp8* apply to inner ear development. During inner ear development, many genes are expressed asymmetrically and orchestrate region-specific development of the inner ear. Although initially uniform, expression of *sp8* becomes restricted

to the dorsal region of the OV, which will give rise to SCC and ED. Loss of *sp8* resulted in otic dysmorphogenesis, similar to mouse mutants of *fgf3*, *mafb*, and *gbx2* (28, 38, 39): absence of ED, abnormal SCC, swelling of the membranous labyrinth, abnormal sensory organs, accompanied by epithelial dilation (Fig. 5), the most common phenotypes of endolymphatic hydrops. The loss of ED in the *ecl* mutant may lead to retention of fluid, enlargement of the OV, and its various consequences as demonstrated in this study. *Grainyhead-like 2* (*grhl2*) mutants in zebrafish (40) showed a range of otic dysmorphogenesis very similar to the *ecl* mutant; however, the molecular mechanism is likely to be dissimilar. Whereas *grhl2* directly regulates epithelial tissue integrity, *sp8* causes more complex effects and the epithelial defects addressed in this study may be a subset of the cause of the defects. Genome sequence data suggest the causative lesion in *ecl* may lie in regulatory elements. Indeed, 5′ genomic sequences of *sp8* contain putative T-cell factor and lymphoid enhancing factor binding elements, conserved sequences of WWCAAG, suggesting that *sp8* expression might be directly regulated by Wnt/β-catenin signaling in the ear. Notably, *wnt* expression is active in the dorsal OV (41) where *sp8* is also expressed, and *sp8* responds to Wnt manipulation (Fig. 5 *O*–*S*). Genetic and embryological analyses in other contexts have revealed that *sp8* reciprocally regulates Fgf signaling (14, 18). Indeed, a recent study has shown that *sp8* is up-regulated by Fgf signaling during otic placode development (42).

Abundant bioinformatic and genetic tools are now available in *X. tropicalis*. The optical clarity of tadpoles at the stage of OV and otoconia formation enables direct observation of inner ear defects. Together our approaches will exploit the full potential of *X. tropicalis* as an inner ear model system, increase knowledge of otic development and otoconia formation, and enhance our understanding of diseases and disorders affecting hearing and balance in vertebrates, including humans.

Materials and Methods

Forward Genetic Screen, Injection, and Imaging. Detailed information is described in *SI Materials and Methods*.

5′ RACE. 5′ RACE was performed using the FirstChoice RLM-RACE kit (Ambion) and 5′ RACE kit (Invitrogen) according to the manufacturers' instructions. *Sp8* sequence information is deposited in GenBank (accession no. KJ158464).

ACKNOWLEDGMENTS. We thank Divya Gupta, supported by the Undergraduate Research Apprentice Program, for her contribution to mapping and R.M.H. laboratory members for helpful discussion. This research was initiated with support from the University of California Berkeley Center for Integrative Genomics and completed with the support of National Institutes of Health's National Institute on Deafness and Other Communication Disorders (R21DC010210 and R01DC011901).

1. Morton CC, Nance WE (2006) Newborn hearing screening—a silent revolution. *N Engl J Med* 354(20):2151–2164.
2. Wu C-C, Chen Y-S, Chen P-J, Hsu C-J (2005) Common clinical features of children with enlarged vestibular aqueduct and Mondini dysplasia. *Laryngoscope* 115(1):132–137.
3. Ladher RK, O'Neill P, Begbie J (2010) From shared lineage to distinct functions: The development of the inner ear and epibranchial placodes. *Development* 137(11): 1777–1785.
4. Chen J, Streit A (2013) Induction of the inner ear: Stepwise specification of otic fate from multipotent progenitors. *Hear Res* 297:3–12.
5. Wallingford JB, et al. (2000) Dishevelled controls cell polarity during Xenopus gastrulation. *Nature* 405(6782):81–85.
6. Hirsch N, et al. (2002) Xenopus tropicalis transgenic lines and their use in the study of embryonic induction. *Dev Dyn* 225(4):522–535.
7. Waldman EH, Castillo A, Collazo A (2007) Ablation studies on the developing inner ear reveal a propensity for mirror duplications. *Dev Dyn* 236(5):1237–1248.
8. Kil S-H, Collazo A (2002) A review of inner ear fate maps and cell lineage studies. *J Neurobiol* 53(2):129–142.
9. Pieper M, Eagleson GW, Wosniok W, Schlosser G (2011) Origin and segregation of cranial placodes in Xenopus laevis. *Dev Biol* 360(2):257–275.
10. Goda T, et al. (2006) Genetic screens for mutations affecting development of Xenopus tropicalis. *PLoS Genet* 2(6):e91.
11. Khokha MK, et al. (2009) Rapid gynogenetic mapping of Xenopus tropicalis mutations to chromosomes. *Dev Dyn* 238(6):1398–46.
12. Hellsten U, et al. (2010) The genome of the Western clawed frog Xenopus tropicalis. *Science* 328(5978):633–636.
13. Harland RM, Grainger RM (2011) Xenopus research: Metamorphosed by genetics and genomics. *Trends Genet* 27(12):507–515.
14. Bell SM, et al. (2003) Sp8 is crucial for limb outgrowth and neuropore closure. *Proc Natl Acad Sci USA* 100(21):12195–12200.
15. Treichel D, Schöck F, Jäckle H, Gruss P, Mansouri A (2003) mBtd is required to maintain signaling during murine limb development. *Genes Dev* 17(21):2630–2635.
16. Griesel G, et al. (2006) Sp8 controls the anteroposterior patterning at the midbrain-hindbrain border. *Development* 133(9):1779–1787.
17. Waclaw RR, et al. (2006) The zinc finger transcription factor Sp8 regulates the generation and diversity of olfactory bulb interneurons. *Neuron* 49(4):503–516.
18. Kawakami Y, et al. (2004) Sp8 and Sp9, two closely related buttonhead-like transcription factors, regulate Fgf8 expression and limb outgrowth in vertebrate embryos. *Development* 131(19):4763–4774.
19. Dickinson K, Leonard J, Baker JC (2006) Genomic profiling of mixer and Sox17beta targets during Xenopus endoderm development. *Dev Dyn* 235(2):368–381.
20. Wells DE, et al. (2011) A genetic map of Xenopus tropicalis. *Dev Biol* 354(1):1–8.
21. Milona MA, Gough JE, Edgar AJ (2004) Genomic structure and cloning of two transcript isoforms of human Sp8. *BMC Genomics* 5:86.
22. Young JJ, et al. (2011) Efficient targeted gene disruption in the soma and germ line of the frog *Xenopus tropicalis* using engineered zinc-finger nucleases. *Proc Natl Acad Sci USA* 108(17):7052–7057.
23. Cermak T, et al. (2011) Efficient design and assembly of custom TALEN and other TAL effector-based constructs for DNA targeting. *Nucleic Acids Res* 39(12):e82.
24. Quick QA, Serrano EE (2005) Inner ear formation during the early larval development of Xenopus laevis. *Dev Dyn* 234(3):791–801.
25. Hulander M, et al. (2003) Lack of pendrin expression leads to deafness and expansion of the endolymphatic compartment in inner ears of Foxi1 null mutant mice. *Development* 130(9):2013–2025.
26. Deng M, Pan L, Xie X, Gan L (2010) Requirement for Lmo4 in the vestibular morphogenesis of mouse inner ear. *Dev Biol* 338(1):38–49.
27. Wanner SJ, Miller JR (2007) Regulation of otic vesicle and hair cell stereocilia morphogenesis by Ena/VASP-like (Evl) in Xenopus. *J Cell Sci* 120(Pt 15):2641–2651.
28. Lin Z, Cantos R, Patente M, Wu DK (2005) Gbx2 is required for the morphogenesis of the mouse inner ear: A downstream candidate of hindbrain signaling. *Development* 132(10):2309–2318.
29. Choi VM, Harland RM, Khokha MK (2006) Developmental expression of FoxJ1.2, FoxJ2, and FoxQ1 in Xenopus tropicalis. *Gene Expr Patterns* 6(5):443–447.
30. Yu X, Lau D, Ng CP, Roy S (2011) Cilia-driven fluid flow as an epigenetic cue for otolith biomineralization on sensory hair cells of the inner ear. *Development* 138(3):487–494.
31. Mackereth MD, Kwak S-J, Fritz A, Riley BB (2005) Zebrafish pax8 is required for otic placode induction and plays a redundant role with Pax2 genes in the maintenance of the otic placode. *Development* 132(2):371–382.
32. Bouchard M, de Caprona D, Busslinger M, Xu P, Fritzsch B (2010) Pax2 and Pax8 cooperate in mouse inner ear morphogenesis and innervation. *BMC Dev Biol* 10:89.
33. Tallafuss A, et al. (2001) The zebrafish buttonhead-like factor Bts1 is an early regulator of pax2.1 expression during mid-hindbrain development. *Development* 128(20): 4021–4034.
34. Kiernan AE, et al. (2005) Sox2 is required for sensory organ development in the mammalian inner ear. *Nature* 434(7036):1031–1035.
35. Padanad MS, Bhat N, Guo B, Riley BB (2012) Conditions that influence the response to Fgf during otic placode induction. *Dev Biol* 364(1):1–10.
36. Sato N, Meijer L, Skaltsounis L, Greengard P, Brivanlou AH (2004) Maintenance of pluripotency in human and mouse embryonic stem cells through activation of Wnt signaling by a pharmacological GSK-3-specific inhibitor. *Nat Med* 10(1):55–63.
37. Christen B, Rodrigues AMC, Monasterio MB, Roig CF, Izpisua Belmonte JC (2012) Transient downregulation of Bmp signalling induces extra limbs in vertebrates. *Development* 139(14):2557–2565.
38. Choo D, et al. (2006) Molecular mechanisms underlying inner ear patterning defects in kreisler mutants. *Dev Biol* 289(2):308–317.
39. Hatch EP, Noyes CA, Wang X, Wright TJ, Mansour SL (2007) Fgf3 is required for dorsal patterning and morphogenesis of the inner ear epithelium. *Development* 134(20): 3615–3625.
40. Han Y, et al. (2011) Grhl2 deficiency impairs otic development and hearing ability in a zebrafish model of the progressive dominant hearing loss DFNA28. *Hum Mol Genet* 20(16):3213–3226.
41. Riccomagno MM, Takada S, Epstein DJ (2005) Wnt-dependent regulation of inner ear morphogenesis is balanced by the opposing and supporting roles of Shh. *Genes Dev* 19(13):1612–1623.
42. Yang L, et al. (2013) Analysis of FGF-dependent and FGF-independent pathways in otic placode induction. *PLoS ONE* 8(1):e55011.